Delayed plasticity of inhibitory neurons in developing visual cortex

Sunil P. Gandhi[a,1], Yuchio Yanagawa[b], and Michael P. Stryker[a]

[a]Keck Center for Integrative Neuroscience, Department of Physiology, University of California, San Francisco, CA 94143-0444; and [b]Gunma University, 4-2 Aramaki-machi, Maebashi City, Gunma, 371-8510 Japan

Edited by Charles F. Stevens, The Salk Institute for Biological Studies, La Jolla, CA, and approved September 4, 2008 (received for review June 26, 2008)

During postnatal development, altered sensory experience triggers the rapid reorganization of neuronal responses and connections in sensory neocortex. This experience-dependent plasticity is disrupted by reductions of intracortical inhibition. Little is known about how the responses of inhibitory cells themselves change during plasticity. We investigated the time course of inhibitory cell plasticity in mouse primary visual cortex by using functional two-photon microscopy with single-cell resolution and genetic identification of cell type. Initially, local inhibitory and excitatory cells had similar binocular visual response properties, both favoring the contralateral eye. After 2 days of monocular visual deprivation, excitatory cell responses shifted to favor the open eye, whereas inhibitory cells continued to respond more strongly to the deprived eye. By 4 days of deprivation, inhibitory cell responses shifted to match the faster changes in their excitatory counterparts. These findings reveal a dramatic delay in inhibitory cell plasticity. A minimal linear model reveals that the delay in inhibitory cell plasticity potently accelerates Hebbian plasticity in neighboring excitatory neurons. These findings offer a network-level explanation as to how inhibition regulates the experience-dependent plasticity of neocortex.

inhibition | ocular dominance | two-photon microscopy | calcium imaging | cortical plasticity

Temporarily depriving one eye of vision during a critical period in early life triggers a reorganization of visual responses in primary visual cortex (V1) known as ocular dominance plasticity (1). Such monocular deprivation (MD) reduces the strength of neuronal responses driven by the deprived eye while increasing responses driven by the open eye, leading to an overall shift in ocular dominance toward the open eye. Not all cells in V1 undergo ocular dominance changes at the same rate. The supragranular layers of cortex (layers II/III) undergo functional and anatomical changes before the thalamocortical input layer (layer IV), suggesting that a subset of cells may guide plasticity in the rest of V1 (2).

The initiation of ocular dominance plasticity depends critically on the level of cortical inhibition. Genetic reduction of intracortical GABA release blocks the effects of MD that can be restored by local pharmacological enhancement of GABA signaling (3, 4). Accelerating the rate of inhibitory cell maturation leads to a precocious period of plasticity (5). These findings have led to the hypothesis that the excitatory–inhibitory balance must reach some threshold level to initiate plasticity (6). The balance of excitation and inhibition depends not only on the maturity and GABA release of inhibitory neurons but also on their pattern of firing. Little, however, is known about the response properties of inhibitory and excitatory neurons during the course of plasticity.

Here we measure the binocular response properties of inhibitory neurons in mice at single-cell resolution. We determine the changes in these responses produced by monocular deprivation and compare them with the changes in their excitatory neighbors. Using a simple Hebbian model, we demonstrate that the observed time course of inhibitory cell plasticity can explain the requirement for a critical level of inhibition for ocular dominance plasticity.

Results

The first step in our experiments was to target cells specifically in the binocular zone of V1, avoiding the secondary visual cortex (area V2), by using a modified version of a rapid cortical mapping technique based on imaging of intrinsic optical signals (7). The binocular zone of a mouse visual cortex consists of a small region in which neurons respond to stimuli confined to the central 30° of the visual field through both eyes (8). The result of one mapping session is shown in Fig. 1*A*. The boundary between V1 and V2 is known to fall on the lateral side of the binocular zone. We made recordings in the medial half of the binocular zone delineated by intrinsic responses; these responses are therefore guaranteed to be in the binocular zone of V1.

Imaging Responses in Labeled Inhibitory Neurons. To visualize inhibitory neurons directly, we studied GAD67-GFP(Δneo) mice expressing GFP in GABA-synthesizing cells under the control of the endogenous *GAD67* gene promoter (see Fig. 1*B*) (9). We recorded the visual responses of these genetically identified inhibitory neurons together with their excitatory counterparts in vivo by imaging calcium transients in the cell bodies by using two-photon laser scanning microscopy. These somatic calcium signals have been shown to reflect cell spiking activity and not subthreshold signals (10–12). A recently developed extracellular injection technique has made it possible to load all or nearly all neurons in a 200- to 300-μm region of cortex with a cell-permeant version of the calcium indicator Oregon-Green BAPTA-1 (OGB-1) (13, 14). This technique has been applied successfully to the study of neuronal response properties in rodent visual cortex (15–17).

Although OGB-1 and GFP emissions overlap spectrally, we readily identified the GFP-positive cells by analyzing the green and orange components of the fluorescence signal. Fig. 1*B* shows the same set of GFP-positive cells before (*i*) and after (*ii*) calcium indicator loading. A combination of orange and green filtered emission channels in these two images shows that the green GFP signal stands out on top of the green-orange resting calcium indicator fluorescence. Applying independent components analysis (ICA), a blind linear unmixing algorithm, to the dual color images confirmed the post hoc linear separability of the GFP (*iii*) and calcium indicator signals that was apparent by eye. We focused our analysis on cells between 150 and 400 μm below the

Author contributions: S.P.G. and M.P.S. designed research; S.P.G. performed research; Y.Y. contributed new reagents/analytical tools; S.P.G. analyzed data; and S.P.G. and M.P.S. wrote the paper.

The authors declare no conflict of interest.

[1]To whom correspondence should be addressed at: Keck Center for Integrative Neuroscience, Department of Physiology, University of California, 513 Parnassus Avenue, Room HSE-804, San Francisco, CA 94143-0444. E-mail: sunil@phy.ucsf.edu.

This article contains supporting information online at www.pnas.org/cgi/content/full/0806159105/DCSupplemental.

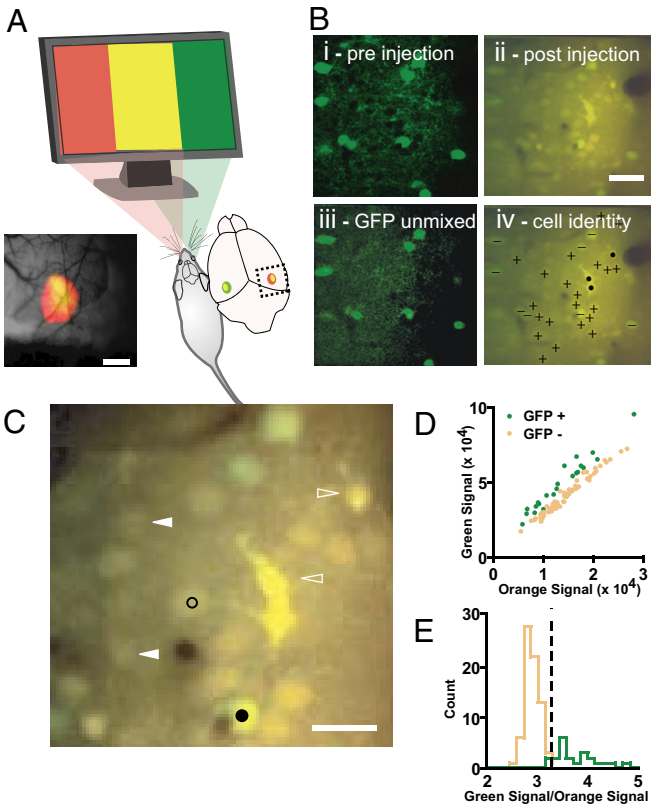

Fig. 1. Identifying inhibitory neurons in the binocular primary visual cortex. (*A*) Intrinsic signal optical imaging reveals the binocular zone of mouse primary visual cortex. Response maps to contralateral eye (in red) and ipsilateral eye (in green) visual stimulation are superimposed. The region of binocular overlap appears as yellow. Subsequent calcium indicator labeling and recording were targeted to the medial half of the mapped binocular region, corresponding to primary visual cortex. (Scale bar: 0.8 mm.) (*B*) Fluorescent signals from GFP-positive inhibitory cells and bulk-loaded calcium indicators are separable. Single plane imaged in two color channels from visual cortex of a mouse line expressing GFP in inhibitory neurons shown before (*i*) and after (*ii*) the extracellular loading of calcium indicator. GFP-positive cells stand out from neuropil and GFP-negative cells. (*iii*) GFP fluorescence is linearly separable from calcium indicator fluorescence after indicator loading. (*iv*) Merged image from *ii* annotated with + symbols for excitatory neurons, − for inhibitory neurons, and ● for astroglia. (Scale bar: 40 μm.) (*C*) Selection of pixels used to measure responses of individual neurons. Circular pixel selections 4 μm wide (examples shown in black; filled is inhibitory and open is excitatory) were drawn within the boundaries of each cell body to guarantee exclusion of neuropil signal contamination. Cell bodies that were poorly sectioned (filled triangles) as well as morphologically identified astroglia (open triangles) were excluded from analysis. (Scale bar: 20 μm.) (*D* and *E*) Neurons identified as GFP-positive before indicator loading (green) are discriminated from GFP-negative neurons (orange) by the ratio of green to orange fluorescence intensity. A discriminator partitions the GFP-positive from GFP-negative neurons (dashed line in *E*).

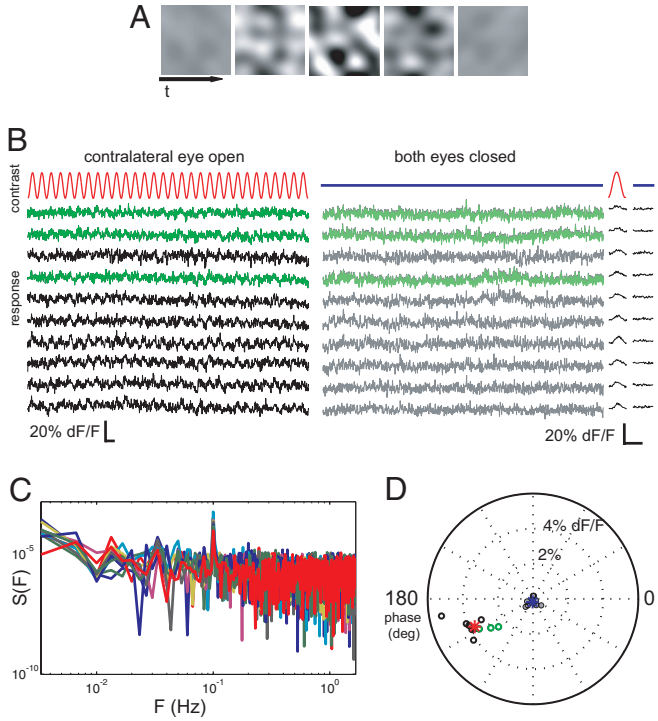

Fig. 2. Measuring cell responses to monocular visual stimulation. (*A*) Contrast modulated stochastic noise visual stimulus. A grayscale movie, modulating sinusoidally between zero and maximal contrast with a 10-s period, was presented separately to each eye (Movie S1 (AVI)). The noise stimulus contained spatial and temporal components tailored to the selectivity of mouse primary visual cortical neurons. (*B*) Example cellular calcium signal traces from 10 simultaneously recorded neurons during 30 cycles of the noise stimulus presented to one eye only (*Left*), or with both eyes occluded (*Right*). Recordings from inhibitory neurons are in green. Time average of 30 cycles plotted for each stimulation condition (far right) shows a periodic response to monocular stimulation in all cells. Scale bars are 20 s (*Left*) and 10 s (*Right*). (*C*) Power spectra of responses to contralateral stimulation show a peak at the fundamental frequency of contrast modulation. (*D*) Responses to visual stimulation are well separated from nonstimulated condition. Shown is a polar plot of the phase and amplitude of the best-fitting sinusoid of period 10 s for each of the cells above in stimulated (open circles) and unstimulated control (filled circles) conditions. Red and blue asterisks indicate the mean response across cells for the stimulated and nonstimulated conditions, respectively. Green circles indicate inhibitory cell responses.

cortical surface, corresponding to the approximate limits of layer II/III in mouse visual cortex (18–21). Cells that were more superficial than 150 μm consisted of sparse layer I neurons. We discarded labeled astrocytes from our analysis based on their morphology (black dots, Fig. 1*Biv*; open triangles, Fig. 1*C*). Cells that were not approximately bisected by the image plane were also discarded (filled triangles, Fig. 1*C*). Black circles in Fig. 1*C* show two examples of the pixels selected to represent individual cells.

We categorized cells as GFP-positive or -negative by summing the fluorescence signal within each cell's selected area and then comparing the summed signal from the two emission channels (Fig. 1 *D* and *E*). A discriminator placed 2.5 σ above the mean green-to-orange signal ratio of GFP-negative cells correctly identifies nearly all (91%) the preidentified GFP-positive cells. By using this discriminator, 21% of all recorded cells were identified as GFP-positive, in close agreement with the fraction of neurons identified as inhibitory (19.5%) found in fixed-tissue histochemical analysis of the Gad67-GFP line (9).

Visual Stimulation of Highly Selective Neurons in Parallel. To measure the monocular visual responses of many cells at once we developed a visual stimulation paradigm. The standard procedure in ocular dominance studies of single cells is first to find a cell's optimal visual stimulus and then to compare the responses to this optimal stimulus when it is presented to each eye separately. This strategy is ill-suited to parallel recording because neurons in mouse visual cortex are highly selective for the orientation and spatial and temporal frequency of the stimulus (18, 19, 22, 23) and because cells with similar stimulus selectivity are not spatially organized (15–17). For example, by using a set of eight oriented drifting gratings whose spatial and temporal characteristics were chosen to excite the largest number of

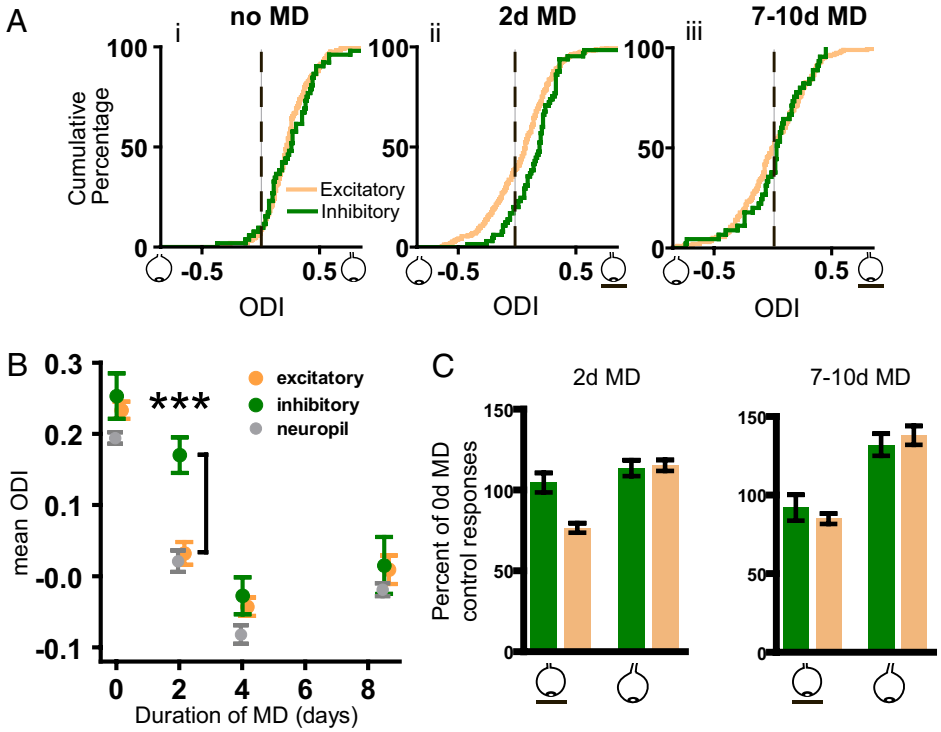

Fig. 3. Monocular deprivation affects excitatory cell responses faster than inhibitory cell responses. (*A*) For each cell, an eye dominance index was computed from the responses to monocular stimulation. The index ranges from −1 for neurons driven exclusively by the ipsilateral eye to +1 for those driven exclusively by the contralateral eye. (*i*) The ODI distributions of inhibitory and excitatory cells responses are similarly biased toward the contralateral eye (K-S test, $D = 0.1356$, $P = 0.382$; $n_{exc} = 253$, $n_{inh} = 52$). (*ii*) After 2 days of monocular visual deprivation (MD) of the contralateral eye, excitatory and inhibitory cell distributions are no longer matched (K-S test, $D = 0.246$, $P = 0.002$; $n_{exc} = 333$, $n_{inh} = 71$). (*iii*) After 7–10 days of deprivation, the two populations are matched again (K-S test, $D = 0.1605$, $P = 0.276$; $n_{exc} = 206$, $n_{inh} = 45$). (*B*) Effect of length of MD on mean ODI for excitatory and inhibitory cells, as well as for the neuropil. Only at 2 days were the inhibitory and excitatory populations significantly different (Mann–Whitney test, $U = 7957$, $P < 0.0001$) as a result of the rapid change in excitatory but not in inhibitory cells. Contamination by neuropil responses cannot account for the delay seen in inhibitory cell plasticity. Error bars reflect standard error of mean. (*C*) (*Left*) Comparison of the median responses from excitatory and inhibitory cells after 2 days of MD, each normalized by the median responses from the control group with no MD. The responses of excitatory cells to the deprived eye are selectively reduced, whereas the deprived-eye responses of inhibitory cells and the open-eye responses in inhibitory and excitatory cells are largely unchanged. (*Right*) After 7–10 d of MD, responses in excitatory cells are similar to those of inhibitory cells, no matter which eye is stimulated. Error bars reflect standard error of the median, obtained by bootstrap estimation.

mouse V1 neurons, each repeated 10 times, we could obtain a reliable response in only 48% of cells (bootstrapped *t* test; $P < 0.01$) [supporting information (SI) Fig. S1 *A* and *B*]. In contrast, recent microelectrode studies reveal that >90% of neurons recorded in layers II, III, and IV are visually responsive, the vast majority quite strongly and selectively (22).

We could find no small set of conventional visual stimuli (bars, spots, gratings, etc) that would activate the entire population of V1 neurons. To stimulate all of the cells in mouse visual cortex, we designed a contrast-modulated stochastic noise stimulus (see Movie S1). The spectrum of the noise stimulus was band limited to match the range of spatial and temporal response properties of mouse V1 cells (22). The contrast of the noise stimulus was modulated sinusoidally from zero to maximal with a 10-s period (see Fig. 2*A* for schematic). In a typical measurement, we presented the noise stimulus to each eye for 5 min (30 cycles). The baseline response of cells (Fig. 2*B*) revealed little obvious spontaneous activity, in agreement with the low spontaneous spiking rates found in single-unit recordings of cells in layer II/III of mouse V1 (22). Nearly all cells responded to the sinusoidal contrast modulation with a periodic response (Fig. 2*B*).

To quantify these periodic visual responses, for each cell we computed the Fourier transform at the fundamental frequency of contrast modulation (see full spectra in Fig. 2*C*), scaled into units of percent fluorescence signal change (Fig. 2*C*). The phase of the fluorescence responses lagged behind the contrast modulation of the noise stimulus by 25°. The lag observed in the responses was expected because the somatic calcium signals measured with OGB-1 temporally filter the underlying spike train with an ≈1-s kernel (11, 12). By using the stochastic noise stimulation technique we were able to obtain significant responses from nearly all cells recorded (99.2%; bootstrapped *t* test, $P < 0.01$). Although the range of noise-evoked response amplitudes (Fig. S2) was lower than the peak signals observed with grating stimulation, we verified that these noise-evoked modulations are driven by large calcium transients (Fig. S3). Furthermore, the relative responses to the two eyes measured by using conventional visual stimulation are strongly correlated with responses to the noise stimulus in the same set of cells ($r^2 = 0.76$; Fig. S1*C*).

Ocular Dominance Plasticity of Inhibitory and Excitatory Neurons. By using the calcium responses to contrast-modulated noise as a measure of each cell's responses to the two eyes and the ability to discriminate inhibitory from excitatory cells, we characterized V1 binocular response properties in normal animals whose ages spanned the critical period for ocular dominance plasticity. Fig. 3*A* shows the distribution of ocular dominance among excitatory and inhibitory cells expressed as the ocular dominance index (ODI). $ODI = (C - I)/(C + I)$, where C and I represent the

measured responses of each cell to the contralateral and ipsilateral eye, respectively. A value of 1 for the ODI indicates a cell exclusively driven by the dominant (contralateral/deprived) eye, a value of −1 indicates a cell driven exclusively by the nondominant (ipsilateral/open) eye, and a value of 0 indicates a cell that responds equally to the two eyes. Initially, excitatory and inhibitory cell responses show similar distributions, with mean ODI values ± SEM of 0.23 ± 0.01 and 0.25 ± 0.03, respectively [Fig. 3*Ai*, Kolmogorov–Smirnov (K-S) test, $D = 0.1356$, $P = 0.382$]. These results agree with those in prior studies of mouse visual cortex (16, 23, 24). Most of the ODI range seen for each population derives from genuine differences among cells in ocular dominance rather than from measurement error (Fig. S4). In contrast, responses from the neuropil between these cells are considerably more homogeneous (Fig. S5).

Next, we examined the ocular dominance of excitatory and inhibitory cells in animals deprived of vision in one eye (monocular deprivation, MD) for various periods. After 2 days of contralateral eye MD, the responses of excitatory cells change dramatically, and the two eyes drive them nearly equally. In contrast, inhibitory neurons remain dominated by the contralateral eye, causing the two populations to diverge sharply. (Fig. 3*Aii*, K-S test, $D = 0.246$, $P = 0.002$). After longer periods of MD, plasticity in inhibitory cells catches up, and their responses again become similar to those of excitatory cells (Fig. 3*Aiii*; K-S test, $D = 0.1605$, $P = 0.276$). Fig. 3*B* plots the time course of the effects of MD on excitatory and inhibitory cells. Whereas the ODI of excitatory cells undergoes a shift toward the open eye that approaches saturation after 2 days MD, the inhibitory ODI is little changed (Fig. 3*B*; Mann–Whitney test for significant difference between excitatory and inhibitory cell ODI at 2 d, $U = 7957$, $P < 0.0001$). By 4 days, the ODI of inhibitory cells has shifted and is realigned with the excitatory population (Fig. 3*B*; Mann–Whitney test, 4-d MD: $U = 3588$, $P = 0.1877$; 7- to 10-d MD: $U = 4197$, $P = 0.5119$).

The main source of potential artifact in the cell responses comes from possible contamination by the surrounding neuropil. Fig. 3*B* plots the ocular dominance of the neuropil signals in addition to those extracted from inhibitory and excitatory cells. The binocular responses in the neuropil track those of the larger and more numerous excitatory cells and are distinct from the slower changes in inhibitory responses. Therefore, it is not possible that contamination from the neuropil accounts for the delayed time course of inhibitory cell plasticity.

It has been observed in other studies of ocular dominance plasticity in mice that the initial effect of MD consists of a 20–30% loss in deprived-eye responses, whereas changes in open eye responses come later and are smaller (16, 25, 26). Normalizing the absolute values of the monocular response measurements for the excitatory and inhibitory cells after 2 days of MD by their corresponding median values before MD reveals that excitatory cells rapidly lose functional input from the deprived eye (Fig. 3*C Left*). Inhibitory cell deprived-eye responses after 2 days MD are as strong as they were initially. In contrast, after 7–10 days of MD (Fig. 3*C Right*), both populations have lost input from the deprived eye and gained input from the open eye.

Model of Ocular Dominance Plasticity. To help understand the functional implications of delayed inhibitory plasticity, we constructed a minimal linear model of Hebbian plasticity consisting of two neurons, one excitatory and one inhibitory, the connections between them, and inputs to each of them serving the two eyes (Fig. 4*A*, equations in *SI Methods*). We used simple differential equations to model the changes in strength of synaptic connections after monocular deprivation. As observed in our experimental findings, the initial inputs provided to each cell are biased toward the contralateral eye identically (see Fig. 3*Ai*). The local excitation of the inhibitory neuron was made weak, in accordance with reports from visual cortical brain slice that superficial layer inhibitory neurons are driven principally by excitatory inputs from cells in other laminae (27–29). Our assumption that inhibitory neurons receive only weak input from local excitatory neurons is also in accord with our experimental finding that the ocular dominance of inhibitory neurons dramatically differs from that of surrounding excitatory neurons after 2 days of monocular deprivation.

When the strength of the deprived-eye input to both the excitatory and inhibitory neurons is reduced while leaving the open-eye input intact, the model (Fig. 4*B*) recapitulates our experimental finding (Fig. 3*C*) of delayed inhibitory cell plasticity. When input from the deprived eye is reduced in the model, the reduction in response of the excitatory neuron to that eye is

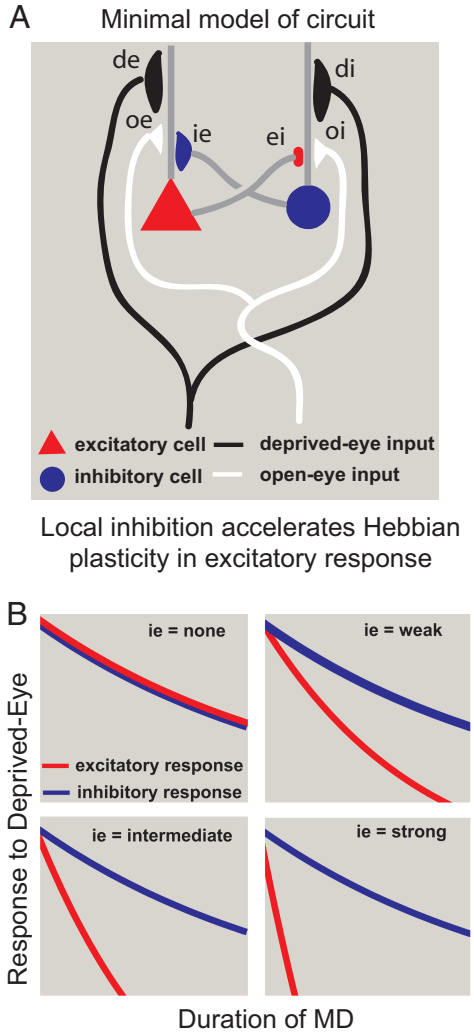

Fig. 4. Possible impact of delayed inhibitory cell plasticity. (*A*) A minimal arrangement of connections to inhibitory and excitatory cells in the upper layers of visual cortex during the critical period that is consistent with our findings and refs. 27–29. Initially, inhibitory and excitatory cells receive similar patterns of inputs from the deprived eye (de = di) and from the open eye (oe = oi). Local excitatory connections onto inhibitory neurons (ei) are not prominent in developing visual cortex. (*B*) A minimal model of Hebbian synaptic modification after monocular deprivation recapitulates the delayed plasticity of inhibitory neurons observed experimentally. On visual deprivation of the contralateral eye, deprived-eye responses from excitatory cells decrease quickly, whereas deprived-eye responses from inhibitory cells fall more slowly. Increasing the strength of local inhibition (ie) alone potently accelerates excitatory cell changes, even when the cell-intrinsic rates of change are equal.

magnified by the inhibition it receives, causing the Hebbian change in the synaptic weight of the deprived-eye input to be more rapid than it would be without such inhibition, and thereby accelerating the change in ocular dominance. The four graphs in Fig. 4*B* show the effect of increasing the local inhibition of the excitatory neuron. The intrinsic plasticities of all of the connections are identical in all graphs. Increasing the strength of local inhibition potently accelerated change in excitatory cell plasticity without requiring intrinsically different plasticities for the two model cells.

The increase of excitatory cell plasticity by strong local inhibition seen in the model depends critically on the assumption of relatively weak local excitation of inhibitory cells. If the inhibitory cells were driven solely by their excitatory neighbors, their binocular responses and plasticity would be identical to those of the excitatory cells.

Our model is limited to explaining only the initial, Hebbian effects of deprivation on deprived-eye responses. A purely Hebbian mechanism could never explain ocular dominance plasticity completely because it would make the deprived-eye responses disappear (30). Recent evidence indicates that the mechanism underlying nondeprived-eye response plasticity is distinct from these Hebbian changes (16, 26, 31–33).

Discussion

In this study we have used functional two-photon imaging at single-cell resolution to identify genetically labeled interneurons and characterize their visual responses. We designed a band-limited noise stimulus that elicits responses in nearly all neurons in mouse visual cortex, allowing the measurement of highly selective neurons whose responses are incompatible with any small set of conventional visual stimuli. We measured the plasticity of responses to the two eyes of upper layer neurons and found that the binocular responses of excitatory neurons change much more rapidly than those of inhibitory neurons. At present, the intrinsic rates of inhibitory and excitatory cell change in plasticity are unknown. Nonetheless, a minimal linear model reveals that accelerated Hebbian plasticity in excitatory neurons is to be expected even if the intrinsic rates are similar for excitatory and inhibitory neurons. Finally, these results provide an explanation for the known requirement of a threshold level of inhibition for normal plasticity in developing visual cortex.

The finding that inhibitory cell plasticity changes more slowly than excitatory cell plasticity was initially surprising. However, in a recent study of plasticity mediated by nucleus basalis stimulation in the adult auditory cortex, excitation and inhibition underwent a similar transient mismatch of response properties, although the mismatch lasted hours instead of days (34). The similarity of our results in developing visual cortex to those in adult auditory cortex suggests that the transient imbalance of local excitatory and inhibitory cells during change may be a general property of cortical circuit reorganization.

This study is consistent with the notion that local connections play an important role in regulating plasticity in visual cortex. Our model shows that increasing local inhibition enhances Hebbian plasticity of the local network. Indeed, one might predict that increasing local inhibition selectively would enhance plasticity even after the end of the normal critical period.

Intraocular TTX injection, lid suture, and dark rearing lead to a wide range of distinct changes in strengths of local connections among neurons in layers IV and II/III and in the intrinsic properties of those neurons in the monocular zone of the rat visual cortex before and at the beginning of the critical period (32, 33). These changes do not account for the delayed plasticity of the visual responses of inhibitory neurons that we find in the binocular cortex *in vivo*. Instead, they could augment the effect of local inhibition on Hebbian plasticity.

The dramatic divergence in plasticity between excitatory and inhibitory neurons raises the possibility that a further subdivision of cortical neurons into functional subclasses may reveal even more profound differences (35). Of specific interest are the responses and plasticity of basket cells, which have been shown to influence the time course of the critical period through experimental alterations of GABA receptors (36). Both the mechanisms responsible for delayed inhibitory cell plasticity and the effects of excitatory–inhibitory mismatch on cortical function may soon become addressable with new tools for the cell-type-specific control of neuronal activity (37).

Materials and Methods

Heterozygous Gad67-GFP(Δneo) mice (9) underwent monocular eyelid suture of the dominant (contralateral) eye at the peak of the critical period (postnatal day 28) for 2, 4, 7, or 10 days. Control (unmanipulated) animals were imaged at ages that spanned the critical period (postnatal days 25–35). Imaging sessions began with intrinsic signal mapping of the binocular zone to locate the binocular portion of the primary visual cortex. Next, calcium indicator solution was pressure injected into the extracellular space at several sites within the binocular zone of V1 (13), targeted ≈250 μm below the brain surface. Approximately 30 min after completion of indicator loading, two-photon calcium imaging began. A 120-μm-wide field-of-view was imaged in time lapse (3.4 Hz) at 820-nm excitation for depths spanning 150–400 μm below the brain surface while the animal viewed a contrast-modulated noise stimulus displayed in the binocular visual field. Each plane in the field of view was imaged continuously for 10 min, while the two eyes were alternately occluded at 5-min intervals. An accompanying cell-type identification image was then obtained by using excitation light (910 nm) better suited for exciting GFP fluorescence.

Animal Preparation and Eyelid Suture. Mice were maintained in the animal facility at the University of California, San Francisco, and used in accordance with protocols approved by the Institutional Animal Care and Use Committee. Gad67-GFP(Δneo) mice were bred into the C57BL/6 background for at least five generations. Only heterozygous animals were used for experiments. For the control group, four unmanipulated animals were imaged at postnatal days 25, 28, 30, and 35. Deprived animals underwent monocular lid suture on postnatal day 28. Eyelid margins were trimmed and eyelids were sutured by using two mattress stitches under isoflurane anesthesia.

Surgical Preparation and Targeted Calcium Indicator Injection. Animals were anesthetized with isoflurane (2.5% induction; 1.5% surgery) in O_2, after a preanesthetic intraperitoneal injection of chlorprothixene (1 mg/kg). Atropine (0.3 mg/kg) and dexamethasone (2 mg/kg) were administered s.c. prophylactically to prevent tracheal secretions and edema, respectively. Core body temperature was maintained at 37.5 °C by using a feedback heating system. EKG and temperature were monitored continuously. Animals were held in place with a post secured to the skull with cyanoacrylate and dental acrylic. In the deprived group, sutures were removed and the eyelid was trimmed. Eyes were washed and coated with a thin layer of silicone oil (30,000 centistokes) to prevent drying. Agarose, 2.5% in extracellular saline (125 mM NaCl, 5 mM KCl, 10 mM D-glucose, 10 mM Hepes, 2 mM $CaCl_2$; pH = 7.4) was applied over the skull, sealed with a coverslip and petroleum jelly. For both intrinsic signal and two-photon imaging sessions, the isoflurane was brought to 0.6–0.8%, which in combination with chlorprothixene was sufficient to keep the animals anesthetized yet to allow robust visual responses. The position of binocular visual cortex was identified by using intrinsic signal imaging (<25 min) as described (8, 26) except that visual stimulation was provided by the contrast-modulated noise stimulus described below. In control experiments, this stimulus delineated the same region as the bar stimulus used previously (8, 26). A craniotomy was cut (<1 mm wide) to expose the binocular zone. Indicator injections were targeted to the medial half of the binocular zone to eliminate the possibility of recording in area V2. Oregon-Green BAPTA-1 acetoxymethyl ester (O-0682, Invitrogen) was dissolved in DMSO and Pluronic F-127 (Invitrogen) and diluted with divalent-ion-free artificial cerebrospinal fluid as per published methods (13). A second dye, Alexa 594 (Invitrogen), whose fluorescence properties do not interfere with calcium indicator or GFP imaging, was included at 1 mM to allow visual monitoring of indicator administration. Calcium indicator was injected under constant 8–12 psi (Picospritzer, General Valve) for 1–2 min through a patch pipette with a tip size of ≈2 μm (inside diameter). A new pipette was used for

each injection. Typically three injections inserted through the intact dura were made per experiment.

Two-Photon Fluorescence Imaging of Cell Identity and Visual Responses. Imaging was performed with a custom-made laser scanning two-photon microscope by using a 16× objective (N.A. = 0.8, CF175, Nikon). Fluorescence imaging for cell identification was excited at 910 nm, whereas calcium imaging was performed with 820-nm excitation (<100 mW). Emissions were split by using a 570-nm longpass dichroic and filtered at 515 ± 25 nm for the green channel and 583 ± 25 nm for the orange channel. Images were acquired by using ScanImage software (38).

Contrast-Modulated Stochastic Noise Stimulus. Visual stimuli were generated by using custom-written scripts in Matlab (Mathworks) by using the Psychophysics Toolbox extensions (39, 40) and displayed on an LCD monitor (Viewsonic VG800b; 60-Hz refresh rate) spanning 52.5 × 70° of visual angle. The stochastic noise movie (Movie S1 (AVI)) consisted of the Fourier-inversion of a randomly generated spatiotemporal spectrum with low-pass spatial and temporal cutoffs applied at 0.05 cycles per degree and 4 Hz, respectively. To provide contrast modulation, the movie was multiplied by a sinusoid with a 10-s period. Movies were generated at 60 × 60 pixels and then smoothly interpolated by the video card to appear 30 × 30 cm on the monitor at a 30-Hz frame rate.

Data Analysis. The cell-type identification image was used to define a 4-μm-diameter region-of-interest (ROI) for each cell. Response traces for each cell were extracted by integrating the fluorescence signal within a ROI across each frame of the time-lapse calcium recordings (3.4 Hz). To calculate the response magnitude for each trace, we took the discrete Fourier transform at the modulation frequency (10 s), projected it onto the average response vector for all cells in a recording session, and scaled it to represent the peak-to-trough percent fluorescence signal change ($\Delta F/F$). The ocular dominance index (ODI) was computed for each cell from the magnitude of the contralateral eye stimulation response, C, and the magnitude of the ipsilateral eye response, I:

$$\mathrm{ODI} = (\mathrm{C} - \mathrm{I})/(\mathrm{C} + \mathrm{I}).$$

We determined the fraction of cells with significant responses to the stochastic noise stimulus and the grating stimulus by using a bootstrap routine for estimating significance thresholds. We repeatedly performed a max operation on either 2 samples (stochastic noise) or 8 samples (grating stimulus) taken from baseline recordings, redrawing samples with replacement, thereby obtaining a new distribution used to derive an estimate of the baseline noise. Analysis of neuropil signals was performed identically to that of cells, including the use of 4-μm ROIs, except that no test was performed to exclude nonsignificant responses.

All image analysis was performed by using custom-written Matlab scripts. Plots were generated in Prism (GraphPad) and Matlab. ICA analysis used the fastICA 2.5 Matlab toolbox (Hyvärinen *et al.*, www.cis.hut.fi/projects/ica/fastica/code/dlcode.html).

ACKNOWLEDGMENTS. We thank R. Froemke for critical discussions, C. Niell for development of the contrast-modulated noise stimulus, and members of the lab for close readings of this manuscript. This work was supported by National Institutes of Health Grants EY02874 and MH077972 (M.P.S.) and EY016317 (S.P.G.) and by Dana Foundation Grant P0001351.

1. Wiesel TN, Hubel DH (1963) Single-cell responses in striate cortex of kittens deprived of vision in one eye. *J Neurophysiol* 26:1003–1017.
2. Trachtenberg JT, Trepel C, Stryker MP (2000) Rapid extragranular plasticity in the absence of thalamocortical plasticity in the developing primary visual cortex. *Science* 287:2029–2032.
3. Hensch TK, *et al*. (1998) Local GABA circuit control of experience-dependent plasticity in developing visual cortex. *Science* 282:1504–1508.
4. Fagiolini M, Hensch TK (2000) Inhibitory threshold for critical-period activation in primary visual cortex. *Nature* 404:183–186.
5. Huang ZJ, *et al.* (1999) BDNF regulates the maturation of inhibition and the critical period of plasticity in mouse visual cortex. *Cell* 98:739–755.
6. Hensch TK (2005) Critical period plasticity in local cortical circuits. *Nat Rev Neurosci* 6:877–888.
7. Cang J, *et al.* (2005) Optical imaging of the intrinsic signal as a measure of cortical plasticity in the mouse. *Vis Neurosci* 22:685–691.
8. Kalatsky VA, Stryker MP (2003) New paradigm for optical imaging: Temporally encoded maps of intrinsic signal. *Neuron* 38:529–545.
9. Tamamaki N, *et al.* (2003) Green fluorescent protein expression and colocalization with calretinin, parvalbumin, and somatostatin in the GAD67-GFP knock-in mouse. *J Comp Neurol* 467:60–79.
10. Smetters DA, Majewska A, Yuste R (1999) Detecting action potentials in neuronal populations with calcium imaging. *Methods* 18:215–221.
11. Kerr JN, Greenberg D, Helmchen F (2005) Imaging input and output of neocortical networks *in vivo*. *Proc Natl Acad Sci USA* 102:14063–14068.
12. Sato TR, *et al.* (2007) The functional microarchitecture of the mouse barrel cortex. *PLoS Biol* 5:e189.
13. Stosiek C, *et al.* (2003) *In vivo* two-photon calcium imaging of neuronal networks. *Proc Natl Acad Sci USA* 100:7319–7324.
14. Garaschuk O, Milos RI, Konnerth A (2006) Targeted bulk-loading of fluorescent indicators for two-photon brain imaging *in vivo*. *Nat Protoc* 1:380–386.
15. Ohki K, *et al*. (2005) Functional imaging with cellular resolution reveals precise micro-architecture in visual cortex. *Nature* 433:597–603.
16. Mrsic-Flogel TD, *et al*. (2007) Homeostatic regulation of eye-specific responses in visual cortex during ocular dominance plasticity. *Neuron* 54:961–972.
17. Sohya K, *et al*. (2007) GABAergic neurons are less selective to stimulus orientation than excitatory neurons in layer II/III of visual cortex, as revealed by in vivo functional Ca^{2+} imaging in transgenic mice. *J Neurosci* 27:2145–2149.
18. Metin C, Godement P, Imbert M (1988) The primary visual cortex in the mouse: Receptive field properties and functional organization. *Exp Brain Res* 69:594–612.
19. Wagor E, Mangini NJ, Pearlman AL (1980) Retinotopic organization of striate and extrastriate visual cortex in the mouse. *J Comp Neurol* 193:187–202.
20. Frost DO, Caviness VS, Jr (1980) Radial organization of thalamic projections to the neocortex in the mouse. *J Comp Neurol* 194:369–393, .
21. Antonini A, Fagiolini M, Stryker MP (1999) Anatomical correlates of functional plasticity in mouse visual cortex. *J Neurosci* 19:4388–4406.
22. Niell CM, Stryker MP(2008) Highly selective receptive fields in mouse visual cortex. *J Neurosci* 28:7520–7536.
23. Drager UC (1975) Receptive fields of single cells and topography in mouse visual cortex. *J Comp Neurol* 160:269–290.
24. Gordon JA, Stryker MP (1996) Experience-dependent plasticity of binocular responses in the primary visual cortex of the mouse. *J Neurosci* 16:3274–3286.
25. Frenkel MY, Bear MF (2004) How monocular deprivation shifts ocular dominance in visual cortex of young mice. *Neuron* 44:917–923.
26. Kaneko M, Hanover JL, England PM, Stryker MP (2008) TrkB kinase required for recovery but not loss of cortical responses following monocular deprivation. *Nat Neurosci* 11:497–504.
27. Dantzker JL, Callaway EM (2000) Laminar sources of synaptic input to cortical inhibitory interneurons and pyramidal neurons. *Nat Neurosci* 3:701–707.
28. Cruikshank SJ, Lewis TJ, Connors BW (2007) Synaptic basis for intense thalamocortical activation of feedforward inhibitory cells in neocortex. *Nat Neurosci* 10:462–468.
29. Yoshimura Y, Callaway EM (2005) Fine-scale specificity of cortical networks depends on inhibitory cell type and connectivity. *Nat Neurosci* 8:1552–1559.
30. Dayan P, Abbott LF (2001) *Theoretical Neuroscience* (MIT Press, Cambridge, MA), 1st Ed.
31. Kaneko M, *et al.* (2008) Tumor necrosis factor-alpha mediates one component of competitive, experience-dependent plasticity in developing visual cortex. *Neuron* 58:673–680.
32. Maffei A, Turrigiano GG (2008) Multiple modes of network homeostasis in visual cortical layer 2/3. *J Neurosci* 28:4377–4384.
33. Maffei A, *et al*. (2006) Potentiation of cortical inhibition by visual deprivation. *Nature* 443:81–84.
34. Froemke RC, Merzenich MM, Schreiner CE (2007) A synaptic memory trace for cortical receptive field plasticity. *Nature* 450:425–429.
35. Markram H, *et al*. (2004) Interneurons of the neocortical inhibitory system. *Nat Rev Neurosci* 5:793–807.
36. Fagiolini M, *et al*. (2004) Specific $GABA_A$ circuits for visual cortical plasticity. *Science* 303:1681–1683.
37. Luo L, Callaway EM, Svoboda K (2008) Genetic dissection of neural circuits. *Neuron* 57:634–660.
38. Pologruto TA, Sabatini BL, Svoboda K (2003) ScanImage: Flexible software for operating laser scanning microscopes. *Biomed Eng Online* 2:13.
39. Brainard DH (1997) The psychophysics toolbox. *Spat Vis* 10:433–436.
40. Pelli DG (1997) The video toolbox software for visual psychophysics: Transforming numbers into movies. *Spat Vis* 10:437–442.